LAWRENCE
LIVERMORE
NATIONAL
LABORATORY

UCRL-TR-211523

Response Of A CVD Diamond Detector To "Typical" Deuterium-Tritium NIF Implosions For Areal Density Measurement

L. S. Dauffy, R. A. Lerche, T. W. Phillips

April 19, 2005

Disclaimer

This document was prepared as an account of work sponsored by an agency of the United States Government. Neither the United States Government nor the University of California nor any of their employees, makes any warranty, express or implied, or assumes any legal liability or responsibility for the accuracy, completeness, or usefulness of any information, apparatus, product, or process disclosed, or represents that its use would not infringe privately owned rights. Reference herein to any specific commercial product, process, or service by trade name, trademark, manufacturer, or otherwise, does not necessarily constitute or imply its endorsement, recommendation, or favoring by the United States Government or the University of California. The views and opinions of authors expressed herein do not necessarily state or reflect those of the United States Government or the University of California, and shall not be used for advertising or product endorsement purposes.

This work was performed under the auspices of the U.S. Department of Energy by University of California, Lawrence Livermore National Laboratory under Contract W-7405-Eng-48.

Response of a CVD diamond detector to "typical" Deuterium-Tritium NIF implosions for areal density measurement.

L.S. Dauffy, R.A. Lerche, T.W. Phillips
Lawrence Livermore National Laboratory, Livermore, CA 94551

Abstract

CVD diamond detector signals from Deuterium-Tritium implosions have been simulated in order to study the feasibility of measuring areal density using the ratio of downscattered to primary neutrons during the ignition campaign at the NIF. Simulated neutron spectra for three "typical" DT implosions were weighted with the CVD diamond sensitivity to obtain an estimated signal at several distances from the target chamber center. The 14 MeV peak was found to have an amplitude about three orders of magnitude larger than the downscattered signal for the three spectra. At a target to detector distance of 17 m (just outside the target bay wall) and for a 1 cm^2 wafer, signals are large enough to be recorded, well above any background and electronic noise. The uncertainty in the areal density measurement comes mainly from the uncertainty in the CVD diamond energy dependent sensitivity, the accuracy of the background simulation, and the effect of the saturation of both detector and electronics after the large 14 MeV peak. Nevertheless, the results found in this study are encouraging, and the remaining sources of uncertainty should now be addressed.

1. Introduction

Advanced nuclear diagnostics are required for the inertial confinement fusion (ICF) ignition campaign at the National Ignition Facility (NIF). High-density and high-temperature plasma is produced during the implosion, releasing strong energetic radiation.[1] The characteristics of the implosion such as neutron yield, areal density (ρR), ion temperature (T_i), and bang time are deduced from measurements of that radiation with different detection systems. Therefore, nuclear diagnostics are crucial for the success of the NIF ignition campaign.

Chemical Vapor Deposition (CVD) diamond wafers are being tested to evaluate the feasibility of measuring areal density by determining the ratio of downscattered to primary neutrons (downscattered neutrons are neutrons scattered inside the target).[1-3] As part of this evaluation, the response of a CVD diamond detector to "typical" Deuterium-Tritium (DT) NIF implosions has been calculated at several distances from target chamber center. The response of the detector was found by weighting the neutron spectra with the sensitivity of the detector. It is important to note that this study did not take into account the electronic noise and the background generated by neutrons and gammas scattered in the chamber and surrounding structures. However, preliminary simulations have found that background to be small.[4]

The feasibility of ρR measurement with a CVD diamond neutron time-of-flight detector remains to be demonstrated. The intensity of the 14 MeV peak is several orders of magnitude larger than the downscattered neutron region, which can lead to difficulties while measuring the spectrum. First, signal saturation by the 14-MeV neutrons may lead to a nonlinear detector response to the downscattered neutrons making accurate signal measurements difficult. Also, the difference of amplitude between the 14 MeV peak and the downscattered neutron region may be too large to be clearly recorded by a saturating oscilloscope. The saturation problem will be addressed in a future report.

2. Typical neutron spectra for NIF implosions

Typical Deuterium-Tritium, DT, implosion neutron spectra were simulated by Steve Haan and have been used as inputs for this study: a 1D clean-burning shot (successful ignition), a 2D fizzle shot (typical failed ignition), and a 1D non-cryo, no pulse shape shot (no ignition). These spectra and normalized spectra versus neutron energy are shown on figure 1. The normalization was done by dividing each channel of the spectrum by the total number of neutrons in the spectrum:

$$\int_0^\infty N_{norm}(E)\,dE = \int_0^\infty \frac{N(E)}{\phi_n}\,dE = 1 \qquad (1)$$

The total neutron yield for each shot, ϕ_n, can be deduced from the energy neutron spectra by calculating the integrals below the curve such as:

$$\phi_n = \int_0^\infty N(E)\,dE = 7.4\ E+18\ \ n \qquad \text{For 1D clean burn shot}$$

$$= 2.1\ E+16\ \ n \qquad \text{For 2D fizzle shot} \tag{2}$$

$$= 5.0\ E+11\ \ n \qquad \text{For 1D non-cryo no pulse shape shot}$$

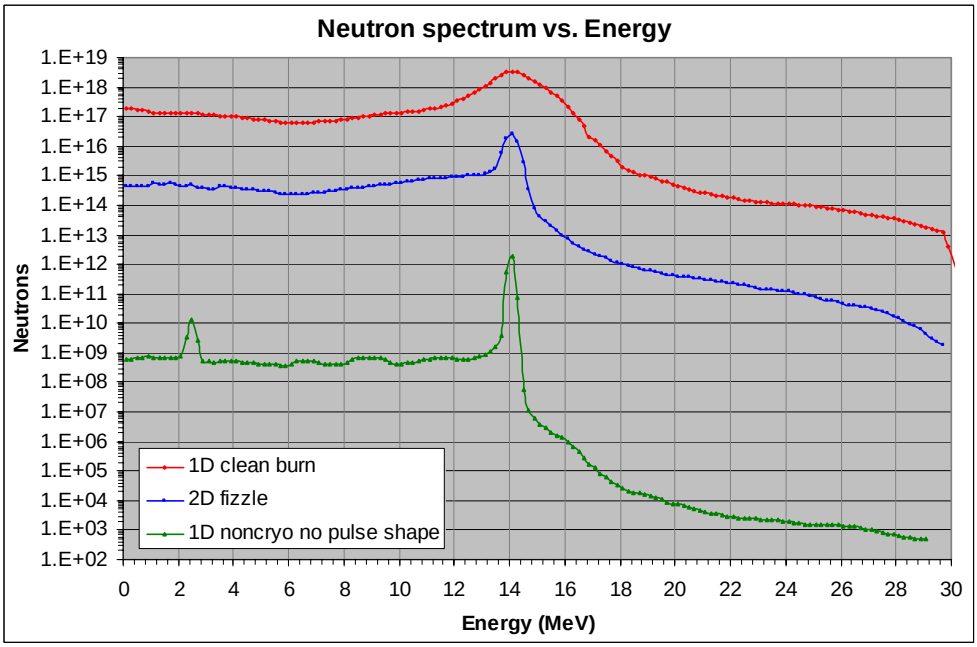

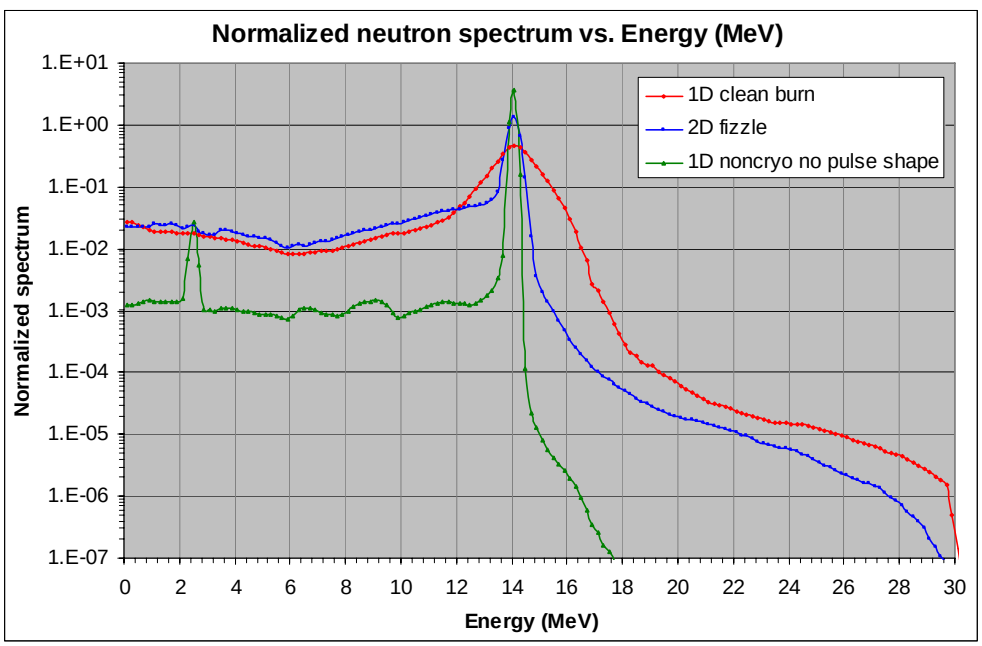

Figure 1. Typical DT implosion neutron spectra and normalized neutron spectra versus neutron energy (area normalized, see text).

3. Conversion from neutron energy spectrum to neutron time-of-flight spectrum

Non-relativistic and relativistic neutron time-of-flight, t, per unit length, L, can be found using the following equations: non-relativistic (equation 3) or relativistic (equation 4).

$$\frac{t}{L} = \sqrt{\frac{m}{2E}} = \frac{1}{c}\sqrt{\frac{mc^2}{2E}} \qquad \text{(from: } E = \tfrac{1}{2}\, mv^2\text{)} \tag{3}$$

$$\frac{t}{L} = \frac{1}{c\sqrt{1-\left(\frac{m_0c^2}{E+m_0c^2}\right)^2}} \qquad \text{(from: } E_{tot} = E + m_oc^2 = mc^2\text{)} \tag{4}$$

The more accurate relativistic equations are used in this study. The error on timing introduced by using non-relativistic equations is - 1.1% at 14 MeV. ICF implosions are nearly point sources in time and space. Thus a neutron distribution versus time-of-flight to a detector can be found from the energy distribution using the relationship between distribution functions:

$$N(E)dE = N(t)dt \tag{5}$$

$$N(t) = N(E)\ dE / dt$$

$$N(t) = N(E)\ \frac{\beta^2}{1-\beta^2}\ \frac{E+m_0c^2}{t} \tag{6}$$

were N(t) is the number of neutrons per unit time, N(E) is the number of neutrons per unit energy (in MeV), L is the detector to target chamber center, TCC, distance in meters, c is the speed of light (2.998 x 10^8 m/s), m_oc^2 is the neutron rest mass equal to 939.566 MeV, and β is a term equal to L/(c*t). From equations 2 and 5 we can deduce that:

$$\phi_n = \int_0^\infty N(E)\, dE = \int_0^\infty N(t)\, dt \tag{7}$$

Figure 2 shows time spectra and normalized time spectra for a distance from target chamber center equal to 1m. The 14 MeV peak is at 19.47 ns. The same spectra are shown for L = 17 m in figure 3. Electronic noise and background spectra resulting from scattering of neutrons on walls and surrounding structures would be added to these spectra at this point, as will be done in future calculations.

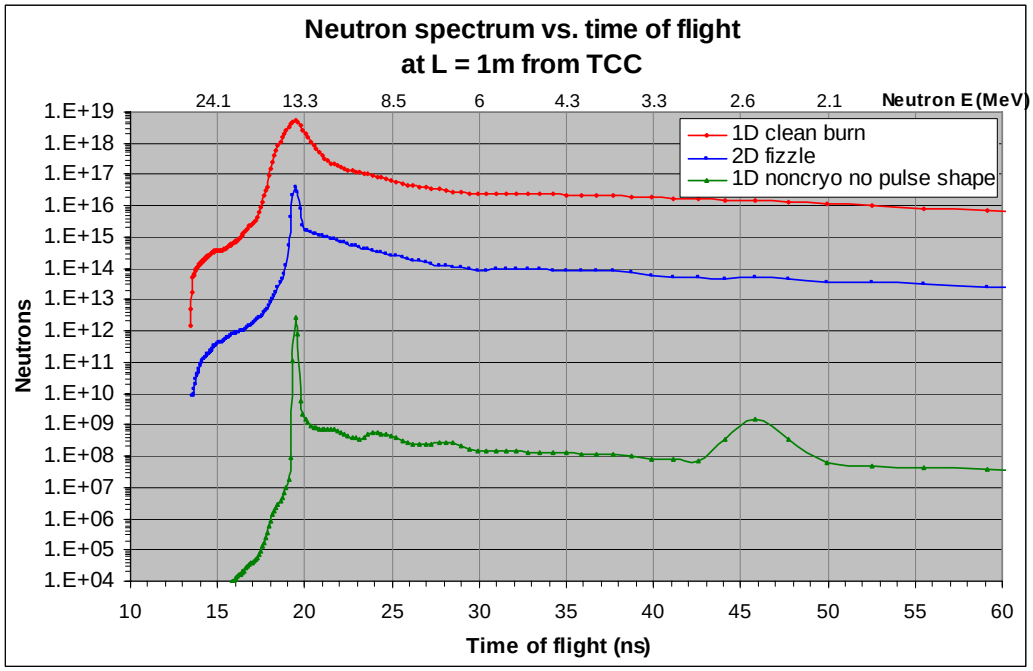

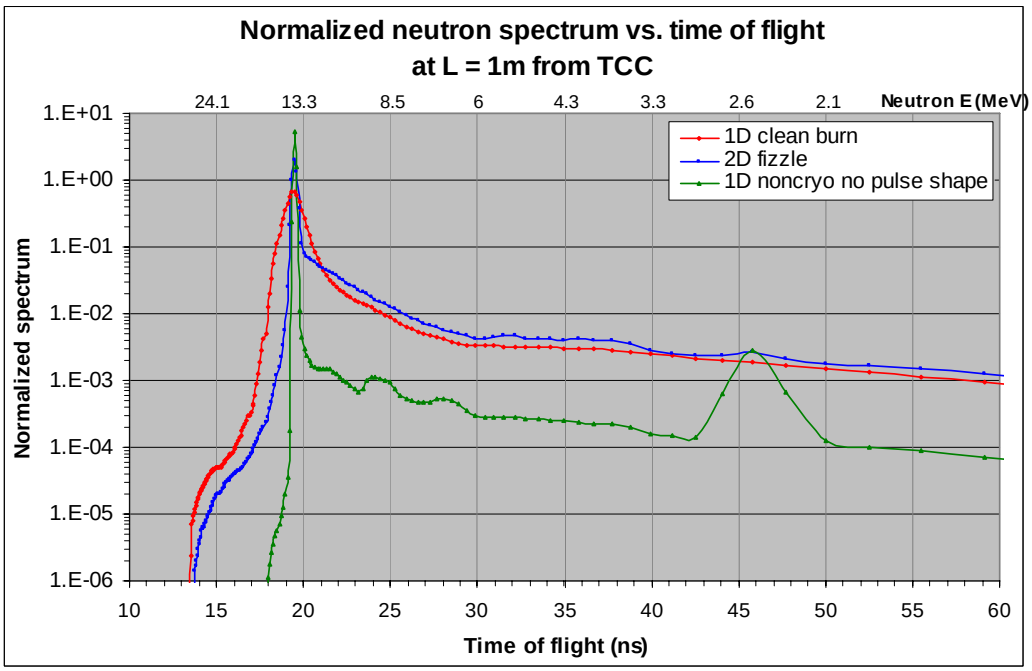

Figure 2. Typical DT implosion neutron spectrum and normalized neutron spectrum versus neutron time-of-flight for L = 1 m. (area normalized).

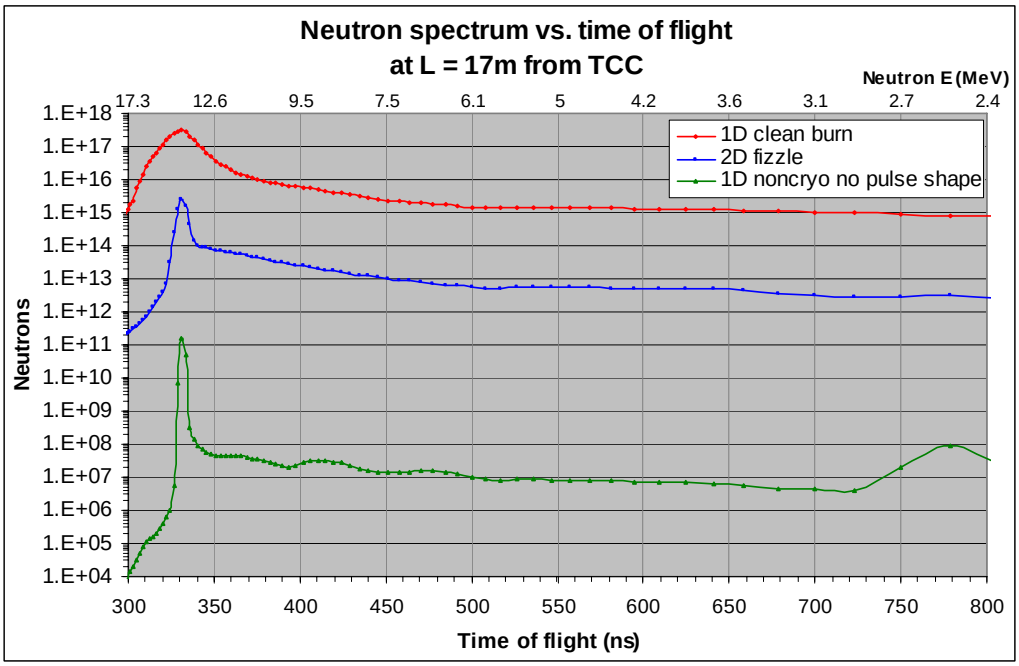

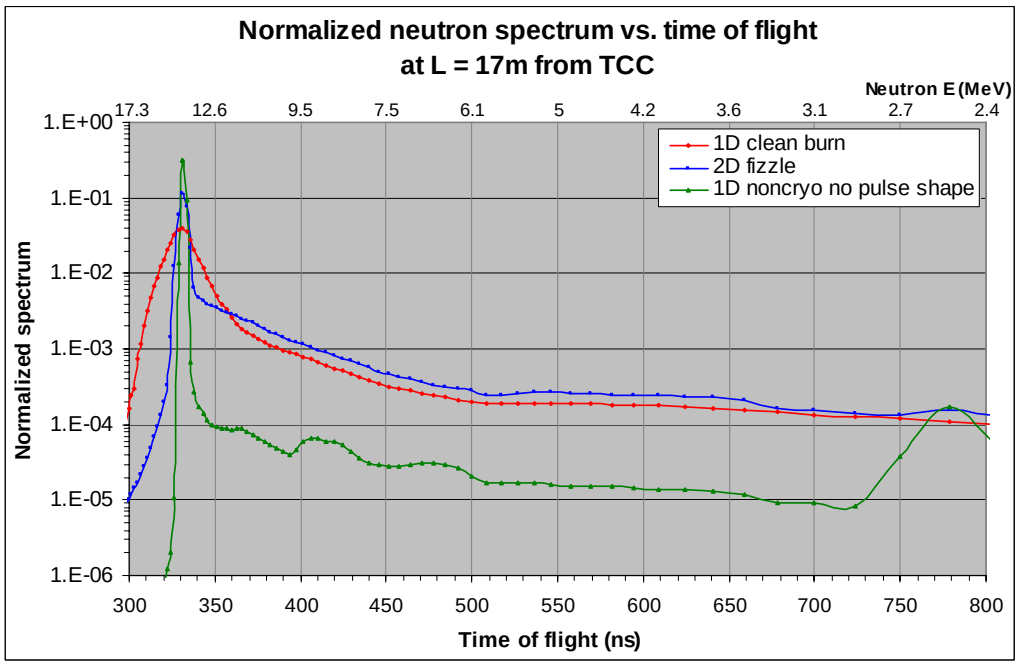

Figure 3. Typical DT implosion neutron spectrum and normalized neutron spectrum versus neutron time-of-flight for L = 17 m. (area normalized).

4. Charge collected in the detector

The charge collected in the wafer, Q in Coulombs, is proportional to the number of electron/hole pairs formed in the crystal:

$$\#e^- = \frac{Q(C)}{1.6*10^{-19}(C/e^-)} \tag{8}$$

This charge can be deduced from the integration of the signal S, $\int S*dt$, using the following equations:

$$\left.\begin{aligned}
S(V) &= R(\Omega)*I(A) &&= R(\Omega)*\frac{Q(C)}{t(s)} \\
Q(C) & &&= 0.02 \quad *S(V)*t(s) \\
Q(\mu C) &= \frac{10^{-9}}{R(\Omega)}*S(\mu V)*t(ns) &&= 2*10^{-11} \quad *S(\mu V)*t(ns) \\
Q(pC) &= \frac{10^{3}}{R(\Omega)}*S(V)*t(ns) &&= 20 \quad *S(V)*t(ns) \\
Q(pC) & &&= 2*10^{-5} \quad *S(\mu V)*t(ns)
\end{aligned}\right\} \tag{9}$$

where R is the resistance of the system and is equal to 50 Ω, I is the current going through the system in Amperes, and the signal S and the time t have the units defined in equation 9.

5. CVD diamond sensitivity to neutrons

The sensitivity of CVD diamonds to neutrons has been calculated by Tom Phillips and is shown on figure 4.[5,6] The two main neutron cross-section libraries have been used for the calculation: the Lawrence Livermore National Laboratory's Evaluated Nuclear Data Library (ENDL) and the Brookhaven National Laboratory's Evaluated Nuclear Data File (ENDF/B IV) libraries.[7,8] In most instances, the ENDF/B data base is more current than ENDL and includes more recent evaluations of new experimental data. ENDL is maintained largely to connect with the data used to analyze integral experiments from the past.

Table 1. Sensitivity, ξ, of a CVD diamond detector for a 1mm thick wafer, an oscilloscope terminated by 50 Ω, E = 1000 V/mm, and for two wafer grades, optical and electronic.[3,9,10]

Neutron energy (MeV)	Optical grade (μV.ns/n)	Electronic grade (μV.ns/n)
2.5	0.24	0.56
14.1	0.62	1.43

Table 1 gives measured values of sensitivities, ξ, for optical and electronic grades of CVD diamond, measured with DD neutrons (2.5 MeV) and DT neutrons (14.1 MeV).[9] The sensitivity curve will vary (scale up and down) depending on the value of the sensitivity measured (given in table 1), which itself depends on the detector thickness, type (optical or electronic grade for example), and voltage bias. In other words, the sensitivity curve must be calibrated with the experimental values of table 1 at a certain neutron energy to get the response of a CVD diamond detector from the original neutron spectra (Steve Haan's data).

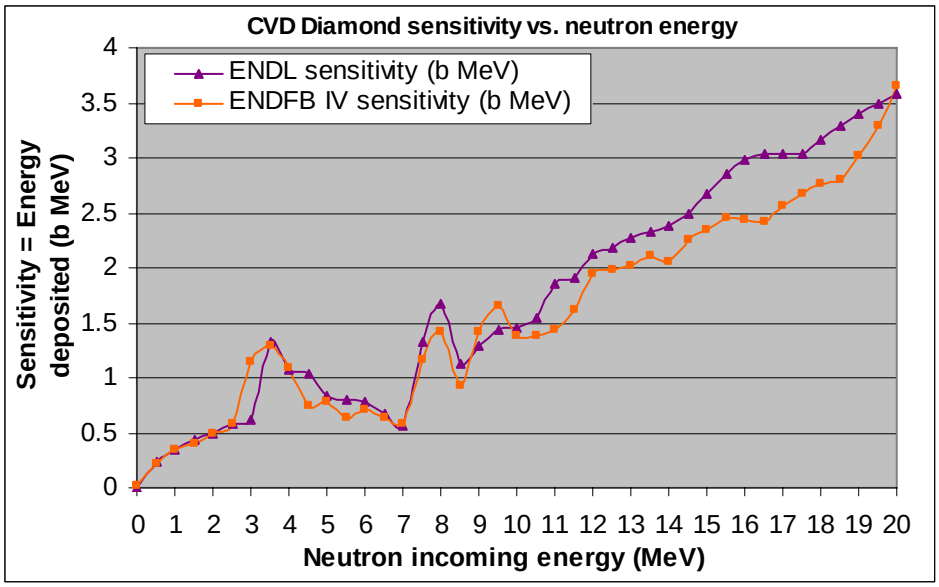

Figure 4. Sensitivity of CVD diamond to neutrons with energies up to 20 MeV ($\Delta E = 0.5$ MeV). Data are for a thin diamond detector, per unit incident neutron.

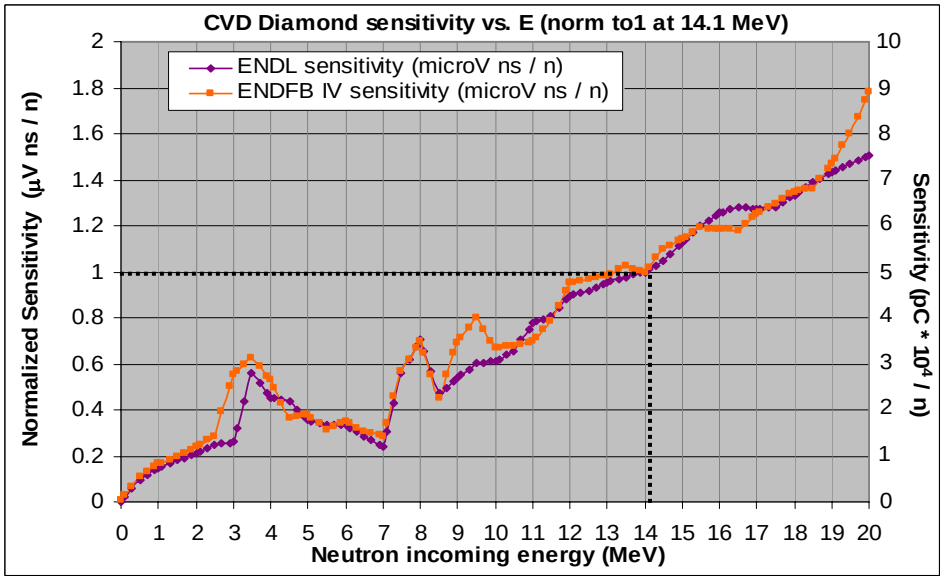

Figure 5a. Sensitivity of CVD diamond to neutrons with energies up to 20 MeV ($\Delta E = 0.2$ MeV), versus incoming neutron energy. Data are per unit incident neutron and for a thin detector.

On figures 5a, the sensitivity curve of figure 4 has been normalized to 1 µV*ns/n at 14.1 Mev, which is close to the real average value of the sensitivity given in table 1 (0.62 + 1.43 / 2). The second unit for the sensitivity, pC/n, is defined in the previous section as $5*10^4$ pC/(µV*ns). Figure 5b shows the same sensitivity curve normalized to 1 µV*ns/n at 19.47 ns, the time-of-flight of a 14.1 MeV neutron corresponding to a detector to target distance of 1 m. The data of figure 4 ($\Delta E = 0.5$ MeV) have been interpolated to fit Steve Haan's energy intervals ($\Delta E = 0.2$ MeV). The sensitivity curve of figure 5a and 5b will be multiplied by the normalized neutron

spectra, respectively versus energy (lower graph of figure 1) and versus time-of-flight (lower graph of figure 2). That will result in the normalized response of the CVD diamond (signal per unit incoming neutron, see following section).

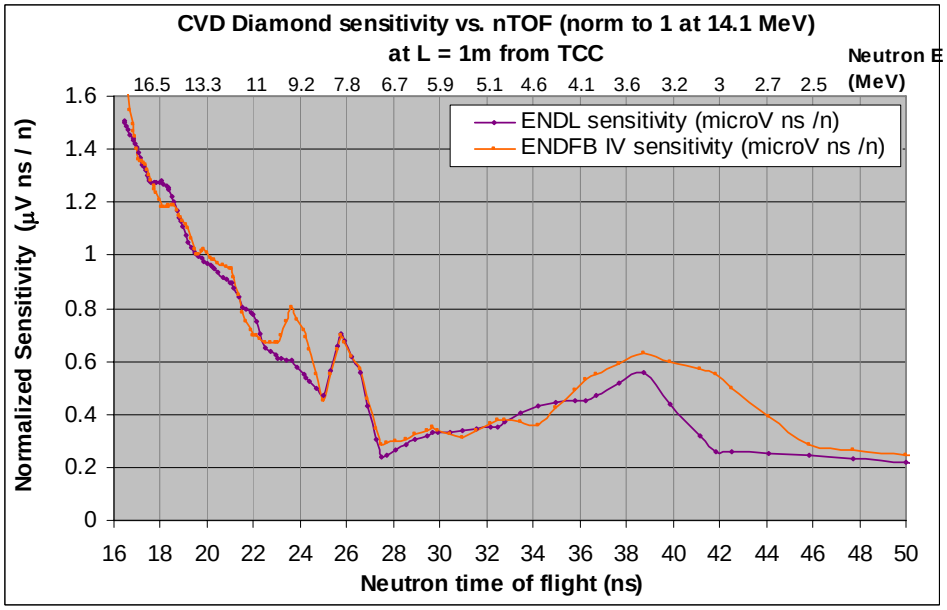

Figure 5b. Sensitivity of CVD diamond to neutrons versus incoming neutron time-of-flight. Data are per unit incident neutron and for a thin detector.

6. Normalized CVD diamond response to "typical" NIF DT implosions

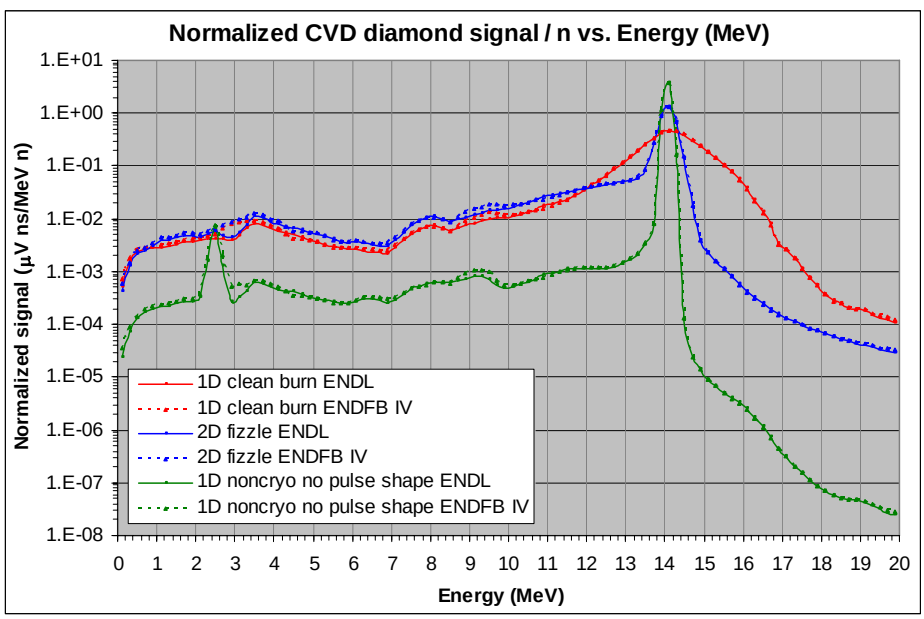

Figure 6. Normalized signals in a CVD diamond detector versus neutron energy in MeV, for 3 "typical" NIF DT implosions and for ENDL and ENDFB IV libraries. Data are per unit incident neutron, for a 1cm^2 detector, and for ξ = 1 µV*ns/n at 14.1 MeV.

As mentioned in the previous section, the normalized neutron spectrum is multiplied point by point by the normalized CVD diamond sensitivity. Sensitivity versus energy (figure 5a) must be used with the energy spectrum (figure 1), and sensitivity versus time (figure 5b) must be used with the time-of-flight spectrum (figure 2). The result is the normalized signal in the CVD diamond detector per unit incident neutron. It is important to note that the term "normalization" refers not only to a sensitivity of 1 at 14.1 MeV, but also to a 1 cm^2 detector area and to a sensitivity per incident neutron. The sensitivity will vary with a larger detector thickness, the nature of the detector (optical or electronic grade for example), and the bias and resistance of the system.

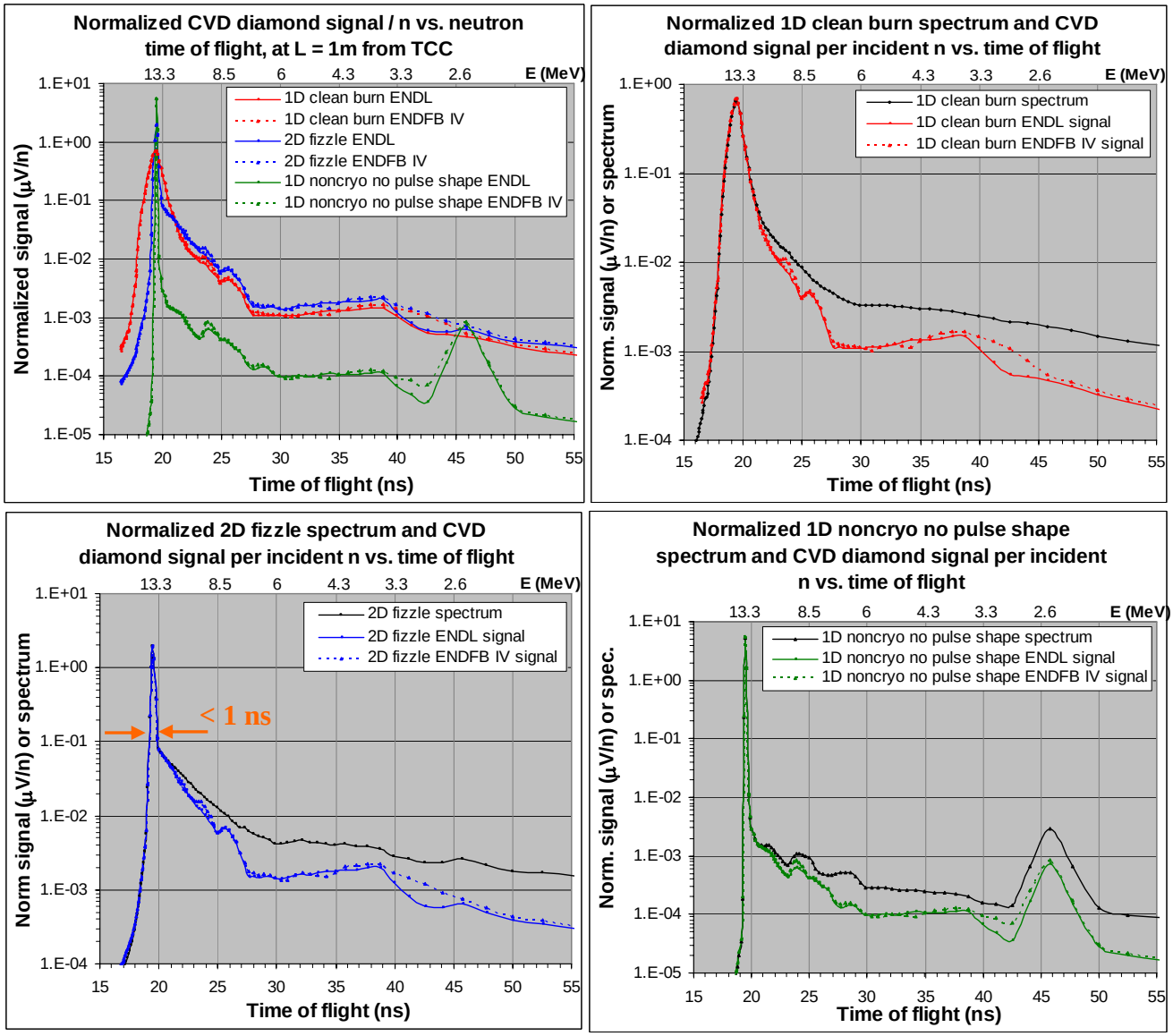

Figure 7. Normalized signals and normalized neutron spectra in a CVD diamond detector versus neutron time-of-flight, at L = 1m, for 3 "typical" NIF implosions and for ENDL and ENDFB IV libraries. Data are per unit incident neutron, for a 1cm^2 detector, and for ξ = 1 μV*ns/n at 14.1 MeV. Figures on the right side and lower left corner are expanded signals.

Figure 6 shows normalized CVD diamond signals versus neutron energy, for the three typical NIF DT implosions. Figure 7 shows these signals versus neutron time-of-flight in ns, at 1 meter from the target chamber center. Normalized neutron spectra from figure 2 are also added to visualize the effect of weighting the neutron spectrum with the CVD diamond sensitivity. Figure 8 represents normalized CVD diamond signals versus neutron time-of-flight at L = 17m.

From a normalized signal at 1 meter, the shape and position of the signal at L(m) can be deduced by doing the following (example for the 2D fizzle shot): time scales with distance, so the 14.1 MeV peak will be at (19.5 ns * L) and its width will be smaller than (1 ns * L). Also the normalized amplitude scales inversely with distance, and the integral below the curve, μV ns /n, will be multiplied by $\phi(n)\ A(cm^2) / 4\ \pi\ L^2\ (cm^2)$.

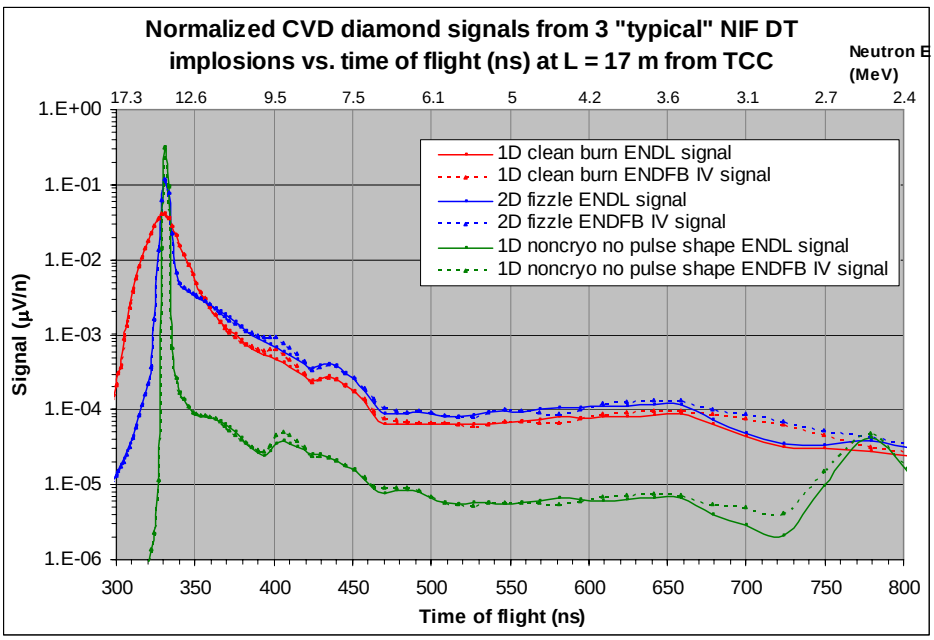

Figure 8. Normalized CVD diamond signals versus neutron time-of-flight, at L = 17m, for 3 "typical" NIF implosions and for ENDL and ENDFB IV libraries. Data are per unit incident neutron, for a $1cm^2$ detector, and for ξ = 1 μV*ns/n at 14.1 MeV.

7. Response of a CVD diamond detector to "typical" NIF DT implosions

The signal in the CVD diamond, S, is found by multiplying the normalized signal, S_{norm}, by the number of incident neutrons on the surface of the detector.

$$S(\mu V) = S_{norm}\left(\frac{\mu V}{n}\right) * \frac{\phi(n)\ A(cm^2)}{4\ \pi\ L^2(cm^2)} * \xi$$

Initial fluxes $\phi(n)$ are given in section 3. The term A is the surface area of the detector in units of cm^2, and ξ is the sensitivity of the detector given in table 1. Figure 9 shows signals

versus neutron energy and figure 10 shows signals versus neutron time-of-flight for L= 1 m. Figure 11 shows signals versus neutron time-of-flight for L= 17 m.

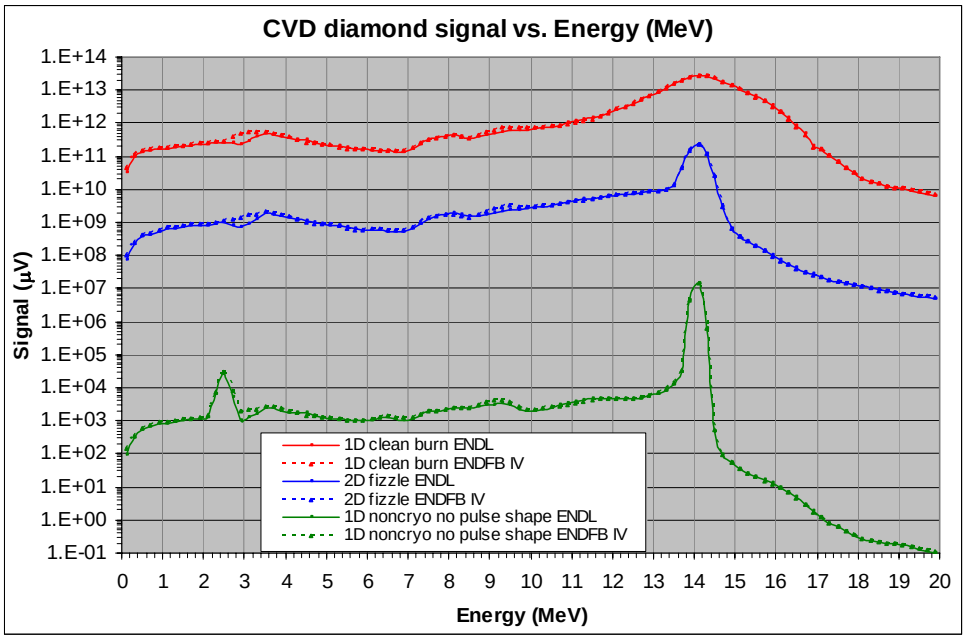

Figure 9. Signals in a CVD diamond detector versus neutron energy, for 3 "typical" NIF implosions and for ENDL and ENDFB IV libraries. Data displayed are for a 1cm^2 detector and for ξ = 1 μV*ns/n at 14.1 MeV.

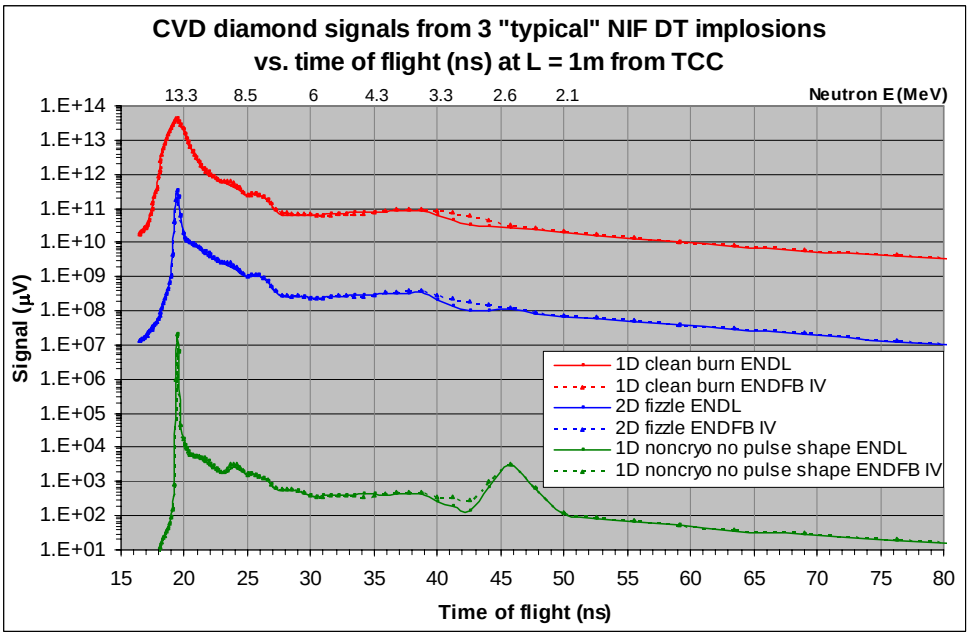

Figure 10. Signals in a CVD diamond detector versus neutron time-of-flight, at L = 1 m, for 3 "typical" NIF implosions and for ENDL and ENDFB IV libraries. Data displayed are for a 1cm^2 detector and for ξ = 1 μV*ns/n at 14.1 MeV.

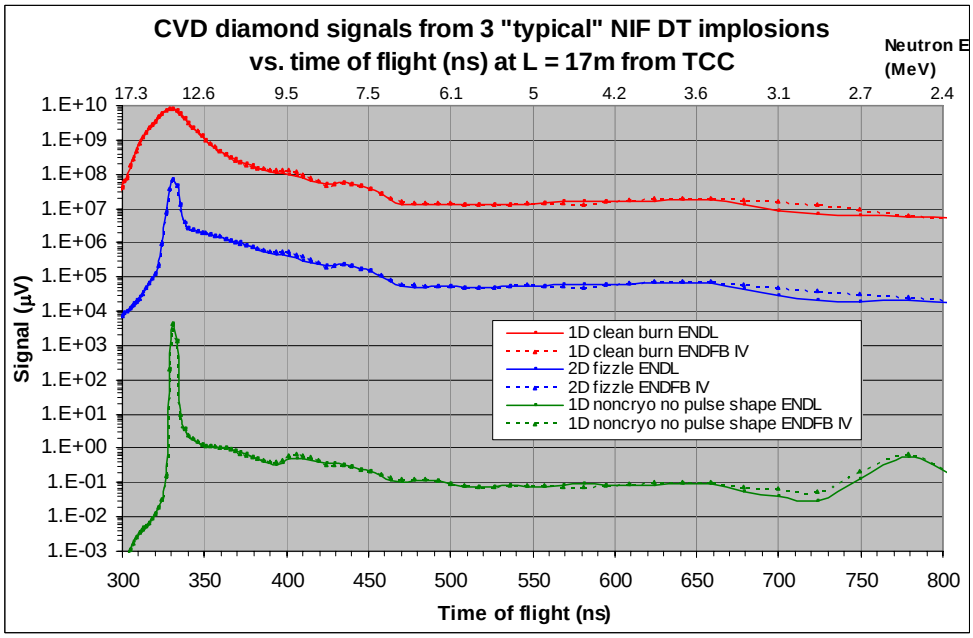

Figure 11. Signals in a CVD diamond detector versus neutron time-of-flight, at L = 17 m, for 3 "typical" NIF implosions and for ENDL and ENDFB IV libraries. Data displayed are for a 1cm^2 detector and for ξ = 1 µV*ns/n at 14.1 MeV.

8. Running integrals

Running integrals of normalized CVD diamond signals have been calculated and are shown on figure 12 (versus neutron energy in MeV) and on figure 13 (versus neutron time-of-flight in ns, for L = 1 m).

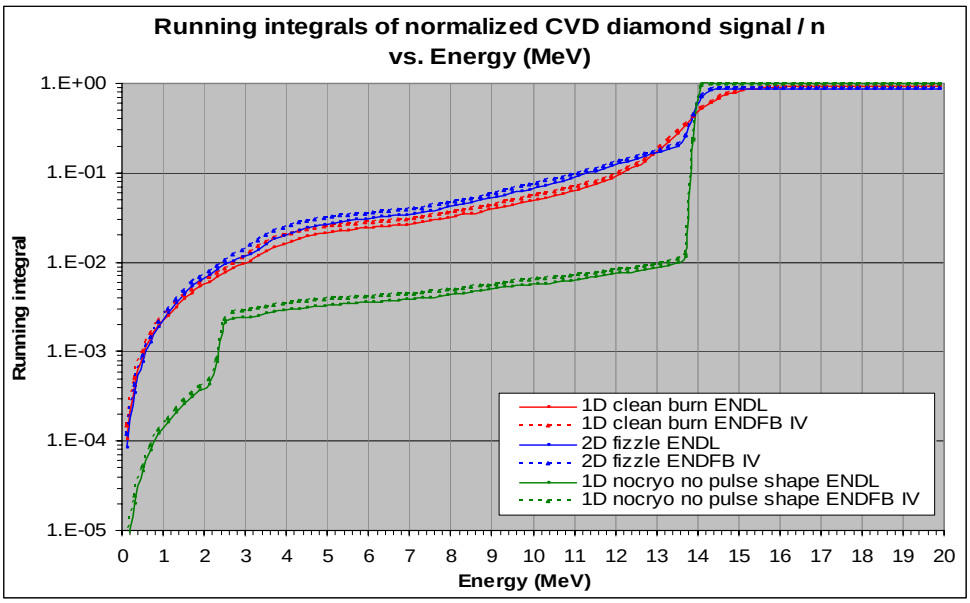

Figure 12 Running integrals of normalized CVD diamond signals versus neutron energy.

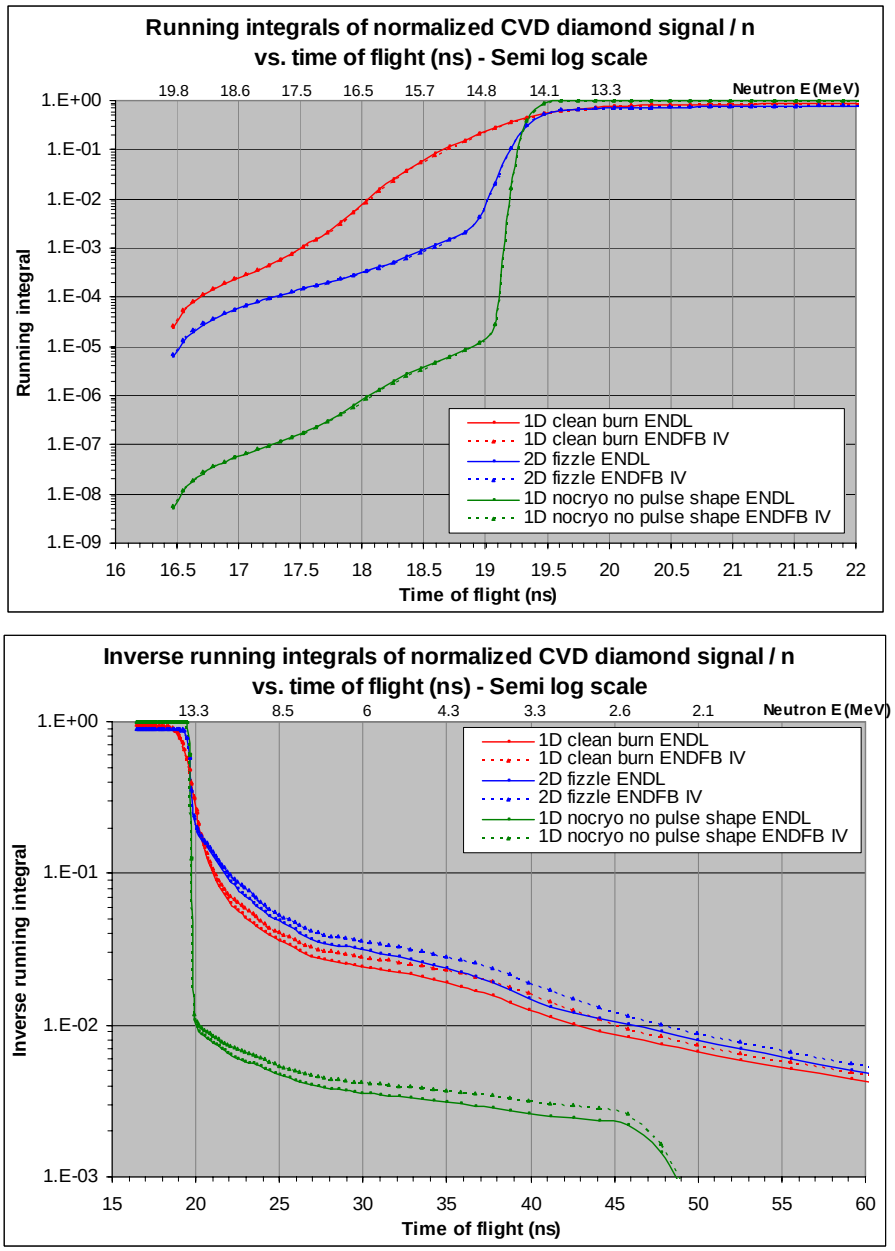

Figure 13 Running integrals and inverse running integrals of normalized CVD diamond signals versus neutron time-of-flight, for L = 1m.

We can see on the upper graph of figure 13 that the majority of the signal is deposited in the CVD diamond in a time of about 3ns. The lower graph of figure 13 shows that the use of a certain neutron cross section library rather than another will add up to 20% uncertainty in the signal in the downscattered region, thus in the ρR value. This graph is also useful to check the size of the downscattered signal compared to the primary neutron signal. For both 1D clean-burning and 2D fizzle shots, the downscattered signal is between 2 and 6% of the primary signal (for a downscattered region taken between 4 and 10 MeV).

9. Analysis and conclusions

The results presented in this report were calculated for a CVD detector with an area of 1 cm^2. No electronic noise and background from neutrons and gamma-rays scattering in the surrounding environment have been added to the incident neutron spectra. Some preliminary background calculations have been done by Peter Song and they showed a low background.

The incident neutron spectra, simulated by Steve Haan, represent three "typical" NIF Deuterium-Tritium implosions (figure 1): a 1D clean-burning shot (successful ignition), a 2D fizzle shot (typical failed ignition), and a 1D non-cryo, no pulse shape shot (no ignition). Relativistic equations have been used for neutron energy to neutron time-of-flight conversion (use of non-relativistic equations would introduced a 1.1% error in the conversion for a 14.1 MeV neutron).

The sensitivity of the CVD diamond was calculated by Tom Phillips using two different neutron cross-section libraries, ENDL and ENDF/B IV. The ENDF/B data base is more current than ENDL and includes more recent evaluations of new experimental data and therefore should be more trusted. It is important to note that the variation in these neutron cross-sections, up to a factor of 2 at some energies (figure 4), will lead to an uncertainty in the simulated signal. This can be seen on the running integrals and inverse running integrals of figures 12 and 13 where a noticeable difference is introduced in the downscattered region (20%), but not in the main 14 MeV peak. This uncertainty will directly affect the value of the areal density. The value of the sensitivity at 2.5 MeV and 14.1 MeV (in units of μV ns per incoming neutron), was measured by Greg Schmid (table 1). The uncertainty on that sensitivity value will have no effect on the ρR measurement, since this is a ratio. The value of this measured sensitivity will vary depending on several factors: thickness of the detector, its nature (optical or electronic grade for example), and the bias and resistance of the system. In conclusion, the main uncertainty in the signal, thus in the areal density value, comes from the uncertainty on the sensitivity curve for the CVD diamond.

A target chamber center to detector distance of 17 meters has been chosen in figures 8 and 11 because it is a possible position for the CVD diamond detector for distant neutron time-of-flight measurement. This is just outside the target bay wall. The amplitudes of the 1D clean burn shot and 2D fizzle shot signals at 17 meters are large enough to be measured, well above any background and electronic noise. They can be easily attenuated to be measured, or alternatively a radiation-hardened diamond could be used.[11-15] The third spectrum (1D non-cryo no pulse shape shot) has a lower amplitude (about 5mV) but it is still possible to see the 14 MeV peak on the oscilloscope, which is what is required for that non-ignition shot since there are no appreciable downscattered neutrons.

The calculated signals (figure 7) present bumps that are due to bumps on the sensitivity curve at 3.5, 8, and 9.5 MeV. That will add uncertainty in the calculation of the number of neutrons in the downscattered region of the signal (4-10 MeV). This uncertainty can be reduced by taking a smaller downscattered region, but can not be avoided completely. Also, there are 3 orders of magnitude between the 14 MeV peak and the downscattered region, and 1 order of magnitude within this downscattered region. So using several channels on the oscilloscope should make the measurement feasible: channel 1 on 1V/div (for the 14 MeV peak), and 1 or 10

mV/div on channel 2 (for the downscattered region). But there will probably be saturation of the oscilloscope after the large 14 MeV peak, leading to a deformed downscattered signal. A gating system that would "hide" the first peak may be a solution. This problem is a serious limitation and should be addressed in future work. The saturation of the CVD diamond wafer is also a problem that should be studied in the future.

10. Acknowledgment

I would like to thank Edward Morse, Jeff Koch, Nobuhiko Izumi, and Vladimir Glebov for their help. This work has been performed under the auspices of U.S. Department of Energy by the University of California Lawrence Livermore National Laboratory under Contract No. W-7405-Eng-48.

11. References

[1]N. Izumi, R. Lerche, M. Moran, T. Phillips, T. Sangster, G. Schmid, M. Stoyer, L. Disdier, J. Bourgade, A. Rouyer, R. Fisher, R. Berggren, S. Caldwell, J. Faulkner, J. Mack, J. Oertel, C. Young, V. Glebov, P. Jaanimagi, D. Meyerhofer, J. Soures, C. Stoeckl, J. Frenje, C. Li, and R. Petrasso, *Nuclear diagnostics of ICF*, Lawrence Livermore National Laboratory, UCRL Report No. UCRL-JC-144322, 2001.

[2]S. Hatchett, "Continued <ρR> diagnostic development for ignition-scale NIF targets," (Lawrence Livermore National Laboratory, 2001).

[3]G. Schmid, V. Glebov, A. Friensehner, D. Hargrove, S. Hatchett, N. Izumi, R. Lerche, T. Phillips, T. Sangster, C. Sibernagel, and C. Stoeckl, "CVD diamond detectors for current mode neutron time-of-flight spectroscopy at OMEGA/NIF," Charged Particle Detection, Diagnostics, and Imaging **4510**, 12-19 (2001).

[4]P. Song "Neutron and gamma-ray background simulation". Private communication. 2005.

[5]T. Phillips, *Calibrating current mode diamond neutron detectors*, Lawrence Livermore National Laboratory, UCRL Report No. UCRL-ABS-205312, 2004.

[6]G. Schmid, J. Koch, M. Moran, T. Phillips, V. Glebov, T. Sangster, C. Stoeckl, S. Wender, and E. Morse, *Calibration of NIF neutron detectors in the energy region E<14 MeV*, Lawrence Livermore National Laboratory, UCRL Report No. UCRL-CONF-203575, 2004.

[7]F. Howerton, D. Cullen, R. Haight, M. MacGregor, S. Perkins, and E. Plechaty, *The LLL Evaluated Nuclear Data Library (ENDL): Evaluation Techniques, Reaction Index, and Descriptions of Individual Reactions*, Lawrence Livermore Scientific laboratory, UCRL Report No. 50400 Vol. 15 Part A, 1975.

[8]R. Kinsey, *Data Formats and Procedures for the Evaluated Nuclear Data File, ENDF*, Brookhaven National Laboratory, Report No. BNL-NCS-50496 (ENDF 102, ENDF/B-V), 1979.

[9]G. Schmid, R. Griffith, N. Izumi, J. Koch, R. Lerche, M. Moran, T. Phillips, R. Turner, V. Glebov, T. Sangster, and C. Stoeckl, "CVD diamond as a high bandwidth neutron detector for inertial confinement fusion diagnostics," REV SCI INSTRUM **74**, 1828-1831 (2003).

[10]G. Schmid, J. Koch, R. Lerche, and M. Moran, "A neutron sensor based on single crystal CVD diamond," NUCL INSTRUM METH A **527**, 554-561 (2004).

[11]W. Adam, E. Berdermann, P. Bergonzo, G. Bertuccio, F. Bogani, E. Borchi, A. Brambilla, M. Bruzzi, C. Colledani, J. Conway, P. D'Angelo, W. Dabrowski, P. Delpierre, A. Deneuville, W. Dulinski, B. van Eijk, A. Fallou, F. Fizzotti, F. Foulon, M. Friedl, K. Gan, E. Gheeraert, G. Hallewell, S. Han, F. Hartjes, J. Hrubec, D. Husson, H. Kagan, D. Kania, J. Kaplon, R. Kass, T. Koeth, M. Krammer, A. Logiudice, R. Lu, L. Mac Lynne, C. Manfredotti, D. Meier, M. Mishina, L. Moroni, J. Noomen, A. Oh, L. Pan, M. Pernicka, A. Peitz, L. Perera, S. Pirollo, M. Procario, J. Riester, S. Roe, L. Rousseau, A. Rudge, J. Russ, S. Sala, M. Sampietro, S. Schnetzer, S. Sciortino, H. Stelzer, R. Stone, B. Suter, R. Tapper, R. Tesarek, W. Trischuk, D. Tromson, E. Vittone, A. Walsh, R. Wedenig, P. Weilhammer, M. Wetstein, C. White, W. Zeuner, M. Zoeller, R. Plano, S. Somalwar, and G. Thomson, "Performance of irradiated CVD diamond micro-strip sensors," NUCL INSTRUM METH A **476**, 706-712 (2002).
[12]L. Allers, A. Howard, J. Hassard, and A. Mainwood, "Neutron damage of CVD diamond," DIAM RELAT MATER **6**, 353-355 (1997).
[13]M. Bruzzi, S. Miglio, S. Pirollo, and S. Sciortino, "Electrical properties and defect analysis of neutron irradiated undoped CVD diamond films," DIAM RELAT MATER **10**, 601-605 (2001).
[14]R. Heidinger, M. Rohde, and R. Sporl, "Neutron irradiation studies on window materials for EC wave systems," FUSION ENG DES **56-7**, 471-476 (2001).
[15]T. Yano, Y. Yamamoto, and T. Iseki, "Physical property change of concurrently neutron-irradiated CVD-diamond, silicon and silicon carbide," J NUCL MATER **307**, 1102-1106 (2002).

Distribution:

NIF:
Nino Landen, L-481
Jeff Koch, L-481
Dick Lerche, L-481
Tom Phillips, L-481
Ed Morse, L-270
Mike Moran, L-481
Nobuhiko Izumi, L-399
Riccardo Tommasini, L-399

CMS:
Tzu-Fang Wang, L-236
Annie B. Kersting, L-231

Laboratory for Laser Energetics, Rochester NY:
Vladimir Glebov